scientific reports

Check for updates

OPEN

Strength hardening and damage mechanism of semiwetted coal under cyclic loads with different initial stress levels

Feixiang Lv[1,2], Yong Zhang[1], Fanjie Kong[2]✉, Xiaobin Li[1] & Quanle Zou[2]

When a coal pillar serves as part of the dam structure in an underground coal mine reservoir, it is subjected to the combined effects of water immersion and dynamic loading. Therefore, understanding the mechanical properties of coal under such conditions is crucial for assessing the stability of underground coal mine reservoirs. While previous studies have investigated the mechanical behavior of coal under cyclic loading conditions, systematic research remains limited regarding structural evolution and mechanical response characteristics under varying initial stress levels in partially saturated environments, particularly for underground reservoir applications. This study investigates the mechanical properties of semi-wetting coal under cyclic loading and unloading at varying initial stress levels, with a focus on stress-strain characteristics, modulus changes, deformation, failure, and energy evolution. The results show that both the strength and the loading/unloading modulus of coal decrease as the initial stress level increases. However, the coal's strength remains higher than its conventional uniaxial compressive strength, indicating a hardening effect due to cyclic loading. This hardening diminishes with higher initial stress levels. Additionally, larger particle sizes and fewer small fragments are observed as initial stress levels rise, suggesting that at lower stress levels, new cracks form but tend to reclose, improving strength and deformation resistance. The cumulative dissipated energy decreases with lower stress levels, highlighting that more energy is required to induce failure at these conditions, further confirming the hardening effect. These findings offer a theoretical foundation for assessing the impact of dynamic loading on coal structure stability under varying initial stress levels.

Keywords Semi-wetting coal, Cyclic loading and unloading, Mechanical properties, Crack closure, Strength hardening

China possesses abundant coal reserves, making coal a fundamental energy source crucial to the development of many industries. For the foreseeable future, coal's position as the primary energy source in China will not change[1,2]. The "Energy Golden Triangle", a key area in China's resource strategy, is characterized by its rich coal deposits and scarce water resources, reflecting the natural endowment of this region. On one hand, coal mining leads to the deformation and fracturing of underground aquifers and aquicludes, causing groundwater loss along fractures and disrupting the regional groundwater balance. On the other hand, coal mining also contributes to water pollution, further exacerbating water scarcity. Thus, conservation and reusee water resources remains a significant challenge for China's coal industry[3,4].

To address the conflict between water resource protection and coal resource development, many scholars have proposed the concept of "guiding, storing, and utilizing" mine water. In this approach, the goaf created by coal mining is utilized as a water storage space, while the protective coal pillar and artificially constructed dam serve as components of the underground reservoir system in coal mines[5–7]. This technology provides a valuable reference for the simultaneous development of coal mining and water resource protection in western mining areas.

Unlike conventional underground reservoirs, the dam structure of a coal mine's underground reservoir consists of both a safety coal pillar and an artificial dam. The coal pillar dam is typically formed from the

[1]State Key Laboratory of Water Resource Protection and Utilization in Coal Mining, National Institute of Low Carbon and Clean Energy, Beijing 102209, China. [2]State Key Laboratory of Coal Mine Disaster Dynamics and Control, School of Resources and Safety Engineering, Chongqing University, Chongqing 400044, China. ✉email: 1016597903@qq.com

remaining coal pillars in the goaf. During coal seam excavation, the coal pillar dam is often subjected to combined disturbances from overburden pressure, water storage pressure, lateral pressure from the goaf rock mass, and dynamic forces caused by large-scale collapses or mine-induced seismic activity (due to mining or goaf rock mass collapse)[8–10]. The initial disturbance stress levels vary depending on environmental factors such as geological conditions and depth of burial.

Moreover, the coal pillar serving as the dam body is generally only partially submerged in water, with the remaining portion exposed to air. As a result, determining the mechanical and deformation failure characteristics of the coal pillar dam under these conditions is challenging, and its stability is crucial to ensuring the safe operation of underground reservoirs[11–13]. Based on this, studying the superposition mechanism of coal under cyclic loading and unloading and semi-wetting conditions at different initial stress levels, as well as its strength, deformation, and failure characteristics, holds significant theoretical and practical importance for the stability and safety of underground reservoir dam construction.

The mechanical strength and deformation failure characteristics of the coal pillar are the decisive factors for the stability of the coal pillar dam of the underground reservoir. The effect of water and stress disturbance in underground reservoir of coal mine is an important condition affecting the characteristics of coal pillar. Scholars at home and abroad have carried out a lot of research on the mechanical and deformation characteristics of coal body according to these two factors. Firstly, water has a significant effect on the mechanical properties of rocks such as coal. Therefore, many researchers have carried out many studies on water-rock interaction in many geotechnical engineering fields[14]. The study of Wong et al. shows that water has a weakening effect on the strength of rocks[15]. Since then, many scholars have analyzed the reasons why water has a weakening effect on rock strength from a deeper perspective. Cai et al. tested the effect of water content on the tensile strength of sandstone through a self-developed tensile device, and found that the tensile strength usually decreases with the increase of water content, and this phenomenon is related to the effect of water on pore pressure and interparticle stress[16]. Wang et al. studied the acoustic emission signals and XRD results of red sandstone under different water contents during shear failure, and explained the weakening effect of water on rock strength from the perspective of the influence of water on the cohesion and internal friction angle of sandstone[17]. In addition, some scholars have further analyzed the interaction between water and rock and the causes of changes in rock brittleness and stiffness from the aspects of energy evolution mechanism, fracture evolution and damage form[18,19]. In addition to the rich achievements in the field of water-rock interaction, some achievements have been made in the study of water-coal interaction. Vishal et al. found that the increase of gas and water in coal samples will reduce the strength of coal samples, and the acoustic emission count will also decrease[20]. By comparing the strength and deformation characteristics of saturated and dry coal samples in uniaxial compression experiments, Perera et al. found that the strength of saturated coal samples decreased while the toughness increased[21]. Through cyclic loading and unloading experiments on coal samples with different water saturation, Pan et al. analyzed the relationship between water saturation and elastic modulus[22].

In addition to the impact of water on the nature of the underground reservoir coal pillar dam, it is also necessary to consider the impact of the stress environment. The coal mine underground reservoir is different from the normal underground reservoir. There may be other mining coal seams near the goaf of the underground reservoir. The adjacent coal seams in the goaf will cause stress disturbance to the goaf during mining operations. Therefore, the coal pillar dam in the underground reservoir of coal mine may often encounter periodic disturbance load, and the strength and deformation characteristics of coal under cyclic load will also affect the stability of coal pillar dam[8,12]. Many studies have shown that the strength and deformation characteristics of coal and other rocks under cyclic disturbance load are different from those under static load[23,24]. Therefore, it is necessary to analyze and discuss the characteristics of coal rock under cyclic disturbance load. Peng et al. conducted fatigue damage experiments on sandstone under cyclic loading with different amplitudes, and found that the change of amplitude would affect the strength and failure mode of sandstone[25]. Meng et al. also studied the effect of cyclic loading at different loading rates on sandstone failure, and pointed out that the release of elastic properties in sandstone is the main reason for rock failure[26]. Song et al. studied the deformation and failure characteristics of sandstone under different cyclic stress levels, and found that the rock was mainly compacted under low stress level, while it was mainly expanded under high stress level[27]. The failure mode of coal under cyclic loading is similar to that of rock, which needs to go through a series of crack compaction, new crack generation, accumulation and penetration. Many scholars have studied the development of this process and achieved some results. Jiang et al. studied the changes of internal cracks in coal samples under cyclic loading through acoustic signals. The results show that the cracks in coal samples increase significantly in the yield stage and increase rapidly in the failure stage. Liang et al. studied the mechanical behavior and failure characteristics of coal under triaxial stepwise cyclic loading and unloading testing. The results show that the failure mode of coal is mainly shear failure, and there is also partial tensile failure[28]. In addition, some scholars also focus on the strength and deformation characteristics of coal pillars under water-bearing conditions in coal mines. Liu et al. studied the stability of water-bearing coal pillars by means of numerical simulation, and found that the lower the water content, the greater the width of the coal pillar, the weaker the sensitivity to stress[29]. Based on the environment of water seepage and mining disturbance, Tan et al. found that resistivity can accurately reflect the damage process of saturated water coal samples by analyzing the damage and damage evolution characteristics of water saturated coal samples under cyclic loading[30]. However, at present, there are few studies on the strength and deformation failure characteristics of coal samples under different initial cyclic stress levels, especially less considering that the coal pillar dam in the underground reservoir of coal mine is usually not completely immersed in water. Therefore, there is a lack of research on the strength and deformation failure characteristics of coal samples under different initial cyclic stress levels under partial infiltration conditions.

Based on the above analysis, there has been considerable research on the mechanical characteristics of coal with varying water content in coal pillar dams and the evolution of the stress field within these dams in

Sample number	Length (mm)	Diameter (mm)	Weight (g)	Wave velocity (km/s)
I-50	100.12	49.96	242.6	1.83
I-60	100.10	49.94	246.2	1.85
I-70	100.08	49.92	243.6	1.87
UCS-1	100.06	49.96	245.9	1.92
UCS-2	99.96	49.98	242.5	1.87

Table 1. Sample parameters.

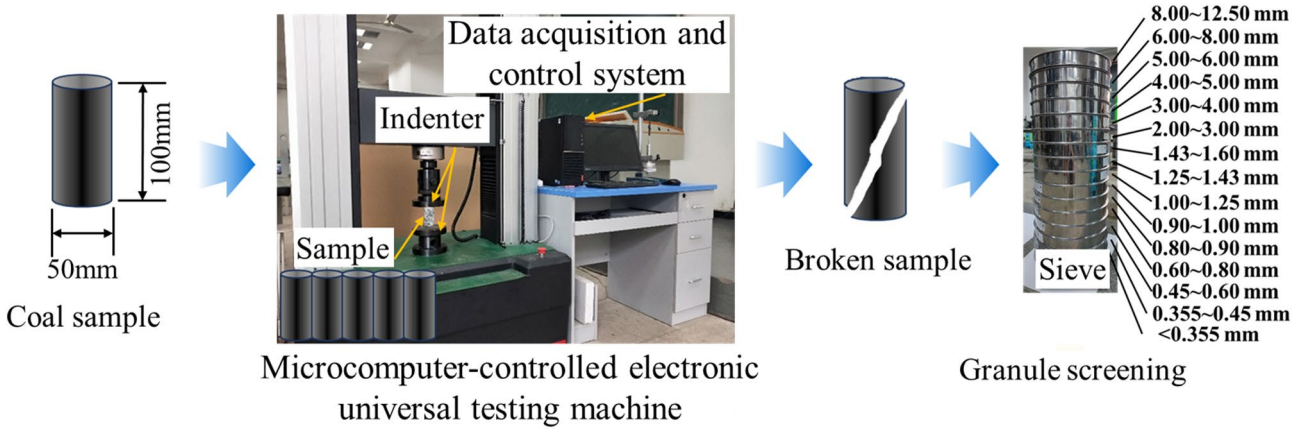

Fig. 1. Schematic diagram of microcomputer controlled electronic universal testing machine.

three-dimensional space. However, while existing studies have investigated the stability of coal pillar dams in underground reservoirs, the majority have examined the effects of individual factors through experimental approaches using fully saturated coal specimens. The mechanical behavior of coal pillar dams in underground reservoirs is fundamentally influenced by their unique operational environment within goaf areas, where adjacent mining activities induce dynamic stress disturbances of varying intensity depending on the relative position of working face advancement, coupled with partial immersion conditions as reservoir water typically covers only the lower portion of the dam structure. To accurately replicate these complex field conditions, our experimental methodology employs a decaying-amplitude cyclic loading path to simulate stress fluctuations during mining operations, combined with a step-increasing stress protocol to capture transitional effects between different working faces, while maintaining controlled semi-immersion at 50 mm water depth to reproduce the characteristic partial saturation state of actual coal pillar dams, thereby achieving both geological realism and experimental precision in our simulations. Therefore, this study aims to investigate the effects of different initial cyclic stress levels and semi-saturation conditions on the strength, deformation, failure, and energy characteristics of coal through cyclic loading experiments on semi-wetting coal specimens.

Experimental samples and schemes

Sample preparation

The coal samples used in this study were all extracted from the same intact coal seam and prepared into cylindrical specimens with a diameter and height ratio of 1:2. In accordance with the ISRM standard[31]. The ends of each specimen were polished to ensure an unevenness of less than 0.02 mm. To reduce effects of inherent variability on mechanical properties of rocks, prepared samples were screened based on their mass and P-wave velocity. Six coal samples with similar mass and wave velocity were ultimately selected. The mass of each coal sample was measured using an electronic balance with an accuracy of 0.01 g, while the length and diameter were measured using a vernier caliper with an accuracy of 0.02 mm. The P-wave velocity was determined using an oscilloscope and a signal generator. The parameters of each sample are presented in Table 1.

Experimental equipment and scheme

The experimental process and treatment measures of semi-wetting coal samples under cyclic loading at different initial stress levels are shown in Fig. 1. The experimental process includes two parts: stepwise cyclic loading and unloading testing and particle size screening. Firstly, the samples were subjected to conventional uniaxial compression and stepwise cyclic loading and unloading testing until the samples were destroyed by the 'servo-controlled universal testing system', and the mechanical parameters such as compressive strength and axial deformation of the samples were tested by the experimental system. The device is driven by a servo motor, and the moving beam is driven up and down by a transmission mechanism to realize the loading of the experimental stress path. To ensure comprehensive fragment recovery during mechanical testing, each coal sample was securely enclosed within a specimen bag prior to loading. Following sample failure, the fractured material was

subjected to systematic particle size analysis using a graded sieve stack arranged in descending order of mesh size (12.5 mm, 25 mm, and 50 mm apertures). Fragment mass distribution was quantitatively determined through precision weighing (± 0.01 g accuracy) of each size fraction, enabling statistically characterization of different particle size ranges.

Before the experiment of cyclic loading, it is necessary to measure the uniaxial compressive strength of this batch of coal samples under conventional loading. Therefore, the uniaxial compressive strength experiment should be carried out by using the samples without soaking treatment. In this section, two samples of UCS-1 and UCS-2 were selected for experiments according to the loading path of Fig. 2a. After that, the average uniaxial compressive strength F_{UCS} of the experimental results of the two samples will be used as the uniaxial compressive strength of this batch of samples and provide a basis for the design of the subsequent stepwise cyclic loading and unloading stress path.

In order to study the stability of coal pillar dam in the actual stress environment of coal mine under different buried depths and other geographical conditions, a mechanical experiment of semi-wetting coal under different initial stress levels was designed. In this experiment, half length of each prepared specimen was soaked in water for twelve hours, while the ambient temperature and humidity were kept constant to simulate 'semi-wetting conditions of retaining wall in dams'. Immediately after immersion, the cyclic loading experiment of the following process was performed on the I-50 coal sample:

(a) Loading at a rate of 400 N s^{-1} to make the axial force reach 50% F_{UCS}.
(b) The coal sample was loaded for 10 min with 50% F_{UCS} as the initial cyclic stress level (I50).
(c) A total of 10 loading and unloading cycles were carried out with 20% F_{UCS} as the amplitude, 1% F_{UCS} as the attenuation value of the upper and lower limits of the cycle, and decreasing step by step.
(d) Retention for 10 min after the end of the cycle.
(e) Loading 10% F_{UCS} again to make the axial force reach 60% F_{UCS}.
(f) Repeat the process described in (b)–(e) above until the coal sample is destroyed. The above loading process is shown in Fig. 2b.

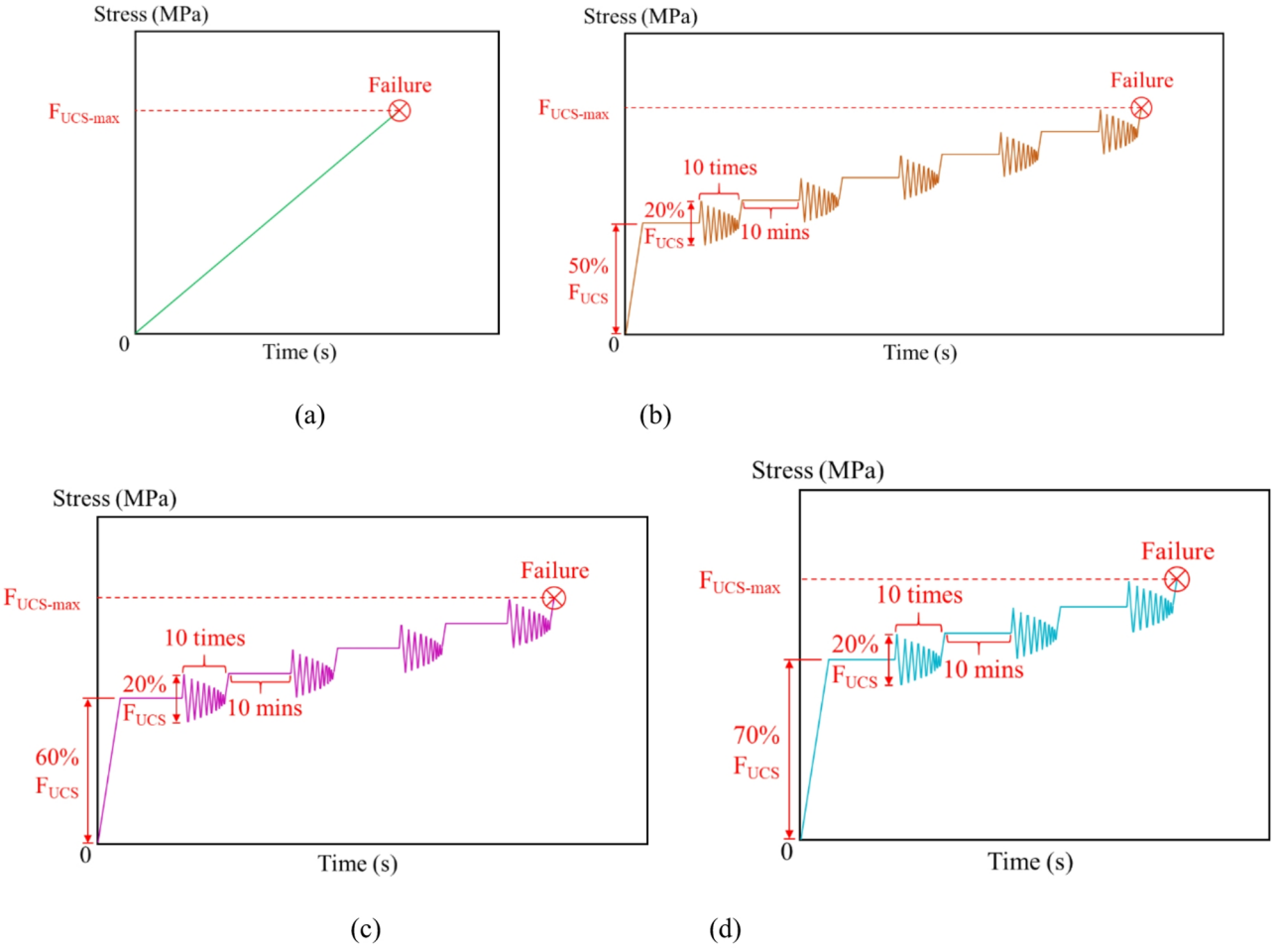

Fig. 2. Loading stress paths. (**a**) Conventional loading. (**b**) 50% F_{UCS}. (**c**) 60% F_{UCS}. (**d**) 70% F_{UCS}.

After that, the above-mentioned stepwise cyclic loading and unloading experiments were carried out on the remaining two water-immersed coal samples I-60 and I-70 with 60% F_{UCS} and 70% F_{UCS} as the initial cyclic stress levels (I_{60}, I_{70}), respectively. The experimental stress paths are shown in Fig. 2c,d.

In the above experimental steps, different initial cyclic stress levels are used to represent different coal mine burial depths, geological conditions and other factors, while the cyclic loading and unloading and holding stages of the attenuation wave form are used to simulate different degrees of engineering activities in the actual mine and the stress environment under the shutdown state.

Results and discussion

Characteristics of stress–strain curves

Through real-time monitoring of a conventional uniaxial compression experiment on two coal samples and a stepwise cyclic loading and unloading experiment on three soaked coal samples, five sets of stress-strain curves were obtained, as shown in Figs. 3 and 4. Figure 3 presents the results of the conventional uniaxial compression tests for the two coal samples, UCS-1 and UCS-2, which have uniaxial compressive strengths of 18.738 MPa and 18.696 MPa, respectively. Based on these results, the average uniaxial compressive strength (F_{UCS}) for this group of coal samples is determined to be 18.717 MPa. Figure 4 shows the stress–strain curves of three soaked coal samples under cyclic loading and unloading conditions with different initial stress levels, along with the variations in uniaxial compressive strength among the coal samples. The stress–strain curves of the coal samples are generally similar. As shown in Fig. 4a, the initial cyclic stress levels for coal samples I-50, I-60, and I-70 are 50%, 60%, and 70% of F_{UCS}, respectively. Their corresponding peak stresses of 20.963 MPa, 20.830 MPa, and 19.055 MPa represent increases of 12.0%, 11.3%, and 1.8% relative to the uniaxial compressive strength (18.717 MPa) of the original coal samples, respectively.

According to Fig. 4b, the uniaxial compressive strength of the coal samples increases under the combined effects of soaking and cyclic disturbance loading. However, when the initial cyclic stress increases from I-50 to I-60, the uniaxial compressive strength of the coal samples decreases slightly. As the initial cyclic stress increases further from I-60 to I-70, a more significant reduction in uniaxial compressive strength is observed. Previous research indicates that varying degrees of water immersion weaken the strength of coal, while cyclic loading and unloading within certain limits can enhance coal strength[20,32]. In this experiment, the strengthening effect of the cyclic loading stress path is clearly greater than the weakening effect of semi-immersion, with the strengthening effect being predominant.

During each cyclic loading and unloading process, the endpoint of the unloading curve does not coincide with the starting point of the loading curve. This discrepancy is due to the formation of new cracks in the specimen during loading. After stress is unloaded, these cracks do not close, resulting in plastic strain. Within the same cycle, because of this plastic deformation, the unloading curve does not return to the initial loading

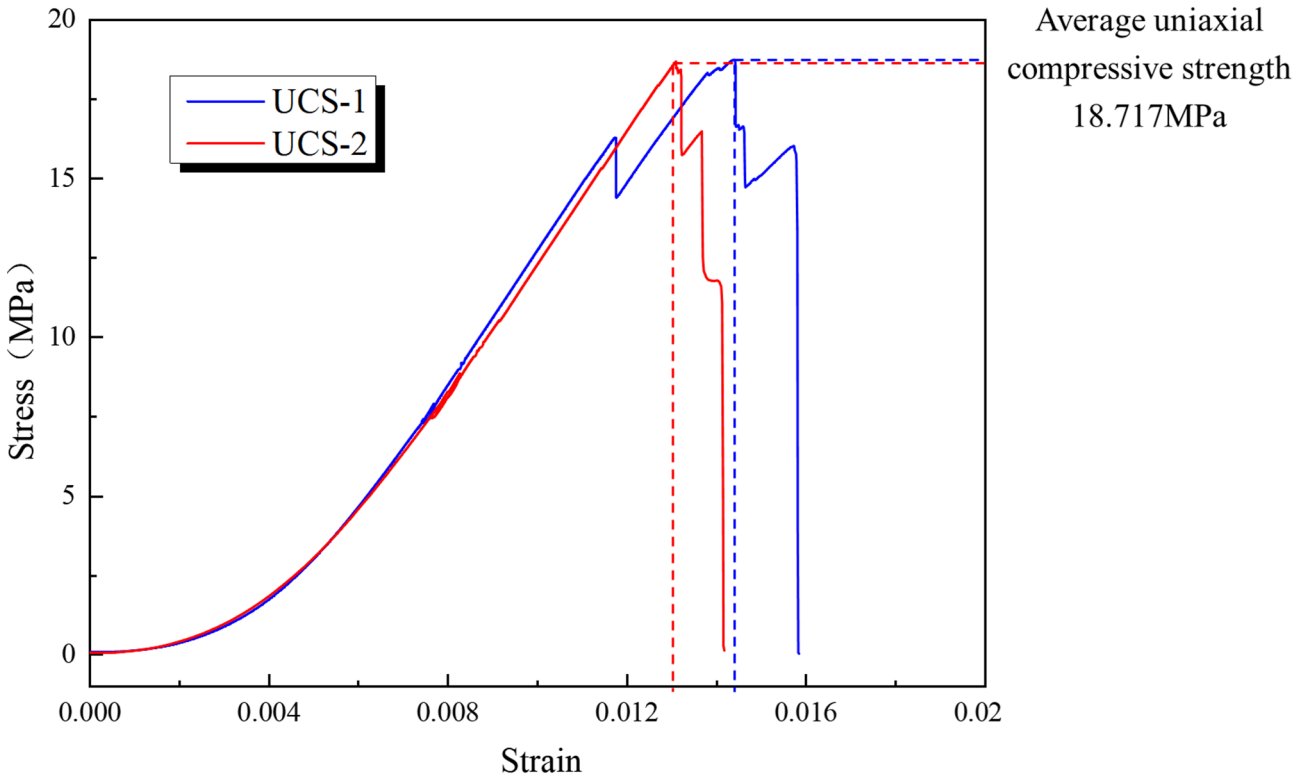

Fig. 3. Stress–strain curve under conventional uniaxial compression.

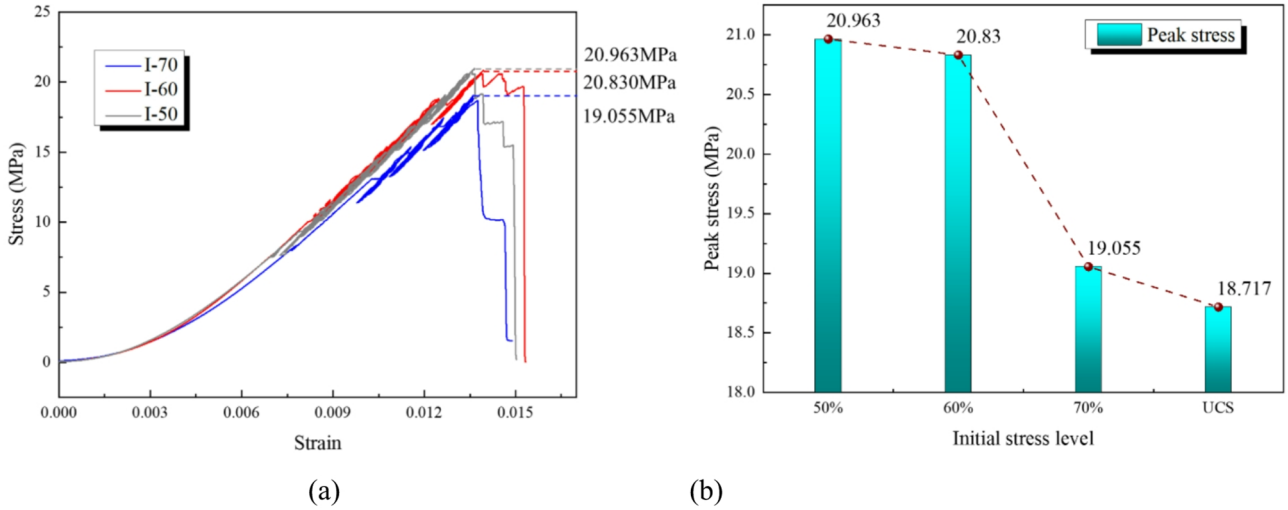

Fig. 4. Stress–strain curves of coal samples under different initial stress levels: (**a**) Stress–strain curves, (**b**) Peak strength of sample under different paths.

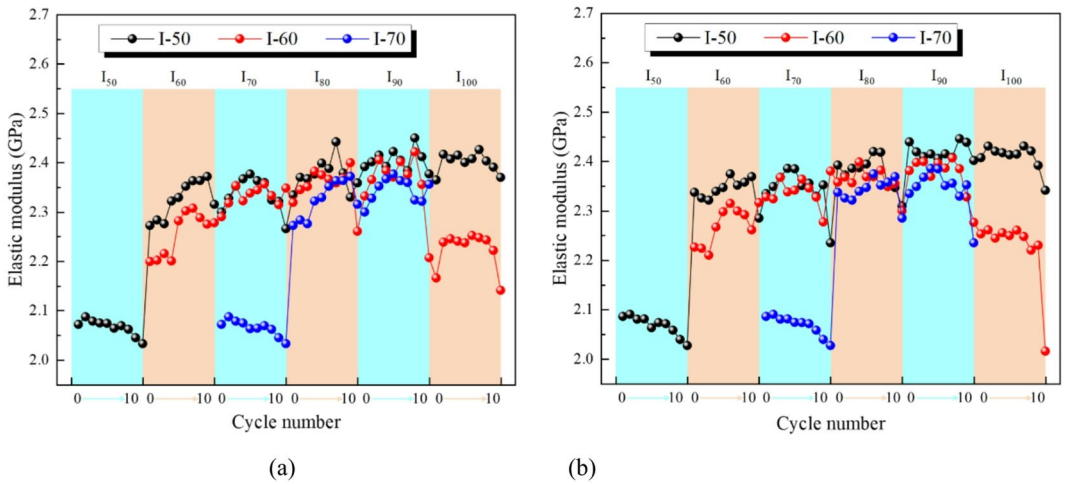

Fig. 5. Elastic moduli of cyclic loading and unloading under different initial stresses: (**a**) Cyclic loading stage, (**b**) Cyclic unloading stage.

state. A hysteresis loop is formed between the loading and unloading curves, and the area of the hysteresis loop is inversely related to the number of cycles.

Loading modulus and unloading modulus

The elastic modulus is a physical quantity that describes the elasticity of a material, generally defined as the ratio of stress to strain in a uniaxial stress state. The changes in the elasticity of coal samples during loading and unloading can be determined by examining the elastic modulus in these stages. In this study, the secant modulus during loading is used as the loading modulus, and the secant modulus during unloading is used as the unloading modulus, both of which are calculated according to the corresponding formulas.

$$E^i = \frac{\sigma^i_{\max} - \sigma^i_{\min}}{\varepsilon^i_{\max} - \varepsilon^i_{\min}} \tag{1}$$

In the formula : E^i is the elastic modulus of the specimen during the i-th cycle, GPa; σ^i_{max} is the upper stress limit of the specimen in the i-th cycle, MPa; σ^i_{min} is the lower stress limit of the specimen in the i-th cycle, MPa; ε^i_{max} is the strain corresponding to the upper stress limit in the i-th cycle; ε^i_{min} is the strain corresponding to the lower stress limit in the i-th cycle.

According to Eq. (1), the elastic modulus of coal samples during the loading and unloading stages under different initial stresses were calculated and plotted, as shown in Fig. 5. It can be observed that the elastic

modulus of coal samples during cyclic loading and unloading ranges between 2.0 GPa and 2.5 GPa. When the initial stress is 50% of F_{UCS}, the loading and unloading elastic moduli in the first cycle show a decreasing trend and are significantly lower than in the subsequent cycles. In the next four cycles, the elastic modulus initially increases and then decreases. During the sixth cycle, the elastic modulus remains relatively stable at the beginning but decreases sharply near failure.

As shown in Fig. 5, the loading and unloading elastic moduli of specimen I-60 during the first four cycles exhibited a trend of initial increase followed by decrease, similar to that observed in the initial cycles of specimen I-50 under its stress path, until the final cycle stage where the moduli first stabilized before showing a significant reduction. Similarly, for specimen I-70, both loading and unloading elastic moduli demonstrated a decreasing trend during the first cycle, while the subsequent two cycles again displayed an initial increase followed by decrease, culminating in a substantial reduction of elastic moduli immediately prior to failure.

It can be observed that the elastic modulus of the coal samples exhibits three distinct stages during the cascade cyclic loading and unloading process. In the first stage, the elastic modulus gradually decreases, typically occurring in the initial cycle. In the second stage, the loading and unloading elastic moduli first increase and then decrease, gradually converging, usually during the middle cycles. This stage indicates that the cracks in the coal sample close under cyclic loading and unloading, and the material properties begin to exhibit elastic characteristics. In the final stage, after reaching a period of stabilization, the elastic modulus of the coal sample decreases significantly. This behavior is attributed to the initial cracks in the coal being compacted under cyclic loading and unloading, leading to an elastic-like response, followed by the formation of numerous new cracks just before failure, causing a rapid decline in the elastic modulus. It should be noted that when the initial stress is 70% of F_{UCS}, the elastic modulus in the last cycle stage of the coal sample does not exhibit stable characteristics. This may be because the initial cracks in the sample are not fully compacted when the number of cycles is too small, meaning the sample has not yet displayed clear elastic behavior.

Additionally, by comparing the loading and unloading elastic moduli of several groups of coal samples, it can be observed that as the initial cyclic stress level increases, the overall elastic modulus during both loading and unloading stages decreases. This phenomenon suggests that an increase in the initial cyclic stress level reduces the coal sample's ability to resist deformation. The lower the initial cyclic stress level of the coal sample, the more low-stress cyclic loading and unloading it undergoes before reaching the same cycle stage, leading to a higher degree of compaction and filling of internal micro-cracks and, consequently, a stronger resistance to deformation.

Deformation and failure characteristics

To obtain the deformation and failure characteristics of coal samples, the strain data from the cyclic loading and unloading stages of the stress-strain curves were processed and calculated. The calculation method is shown in Fig. 6. Using the method provided in Fig. 6, the peak strain (ε^i_{max}), valley strain (ε^i_{min}), median strain (ε^i_{mid}), and irreversible strain of the coal samples were determined. Figure 7 illustrates the peak and valley strains for each loading and unloading cycle during the cyclic loading and unloading stages for three groups of coal samples under different initial stress levels.

Figure 7 illustrates that the peak strain of the coal samples during cyclic loading and unloading decreases with the increasing number of cycles, while the valley strain increases with the number of cycles. This behavior is determined by the stress path of cyclic loading and unloading. As the number of cycles increases, the amplitude of loading and unloading gradually decreases; specifically, the upper limit of cyclic loading and unloading decreases, and the lower limit increases. Therefore, the peak and valley strains of the coal samples follow this trend.

Additionally, by comparing the peak and valley strains of several groups of coal samples, it can be observed that the strain level increases with the initial cyclic stress level. In the previous section, the variation in the elastic modulus of different groups of coal samples and its causes were compared and analyzed, revealing that an increase in the initial cyclic stress level reduces the coal samples' resistance to deformation. The comparison of peak and valley strains among the groups of coal samples in this section is consistent with that conclusion.

Figure 8 presents the median strain for each loading and unloading cycle during the cyclic loading and unloading stages of three groups of coal samples at different initial stress levels. The curves in the figure represent the median strain during the loading stage and the median strain during the unloading stage, respectively. As seen in the figure, both the median strain of loading and unloading increase with the number of cycles and cycle stages. However, compared to the steady increase within each cycle, the median strain exhibits a "jump" or abrupt increase when transitioning to the next cycle. This indicates that the coal sample becomes more susceptible to deformation and failure when the stress level suddenly increases.

Furthermore, the median strain of coal samples with initial stress levels of 50% F_{UCS}, 60% F_{UCS}, and 70% F_{UCS} is 0.01155, 0.01179, and 0.01287, respectively, at the end of the I_{90} cycle stage, and a similar pattern is observed at the end of other cycle stages. These results demonstrate that the ability of coal samples to resist deformation decreases as the initial stress level increases.

Based on the irreversible strain calculation method provided in Fig. 6, the cumulative irreversible strain for each stage can be obtained by summing all the irreversible strains of each cycle stage, as shown in Fig. 9a. Additionally, the cumulative irreversible strain for the entire cycle can be determined by summing the irreversible strains of all stages, as shown in Fig. 9b.

As seen in Fig. 9a, the irreversible strain of the three groups of coal samples increases with the initial stress level in the same cycle stage, with a more pronounced increase in the failure stage. This phenomenon indicates that as the initial stress level increases, the coal samples exhibit greater brittleness at each cycle stage, resulting in more severe deformation during failure. Furthermore, in the failure stage, the irreversible strain of the coal samples increases significantly, which may help predict coal sample failure.

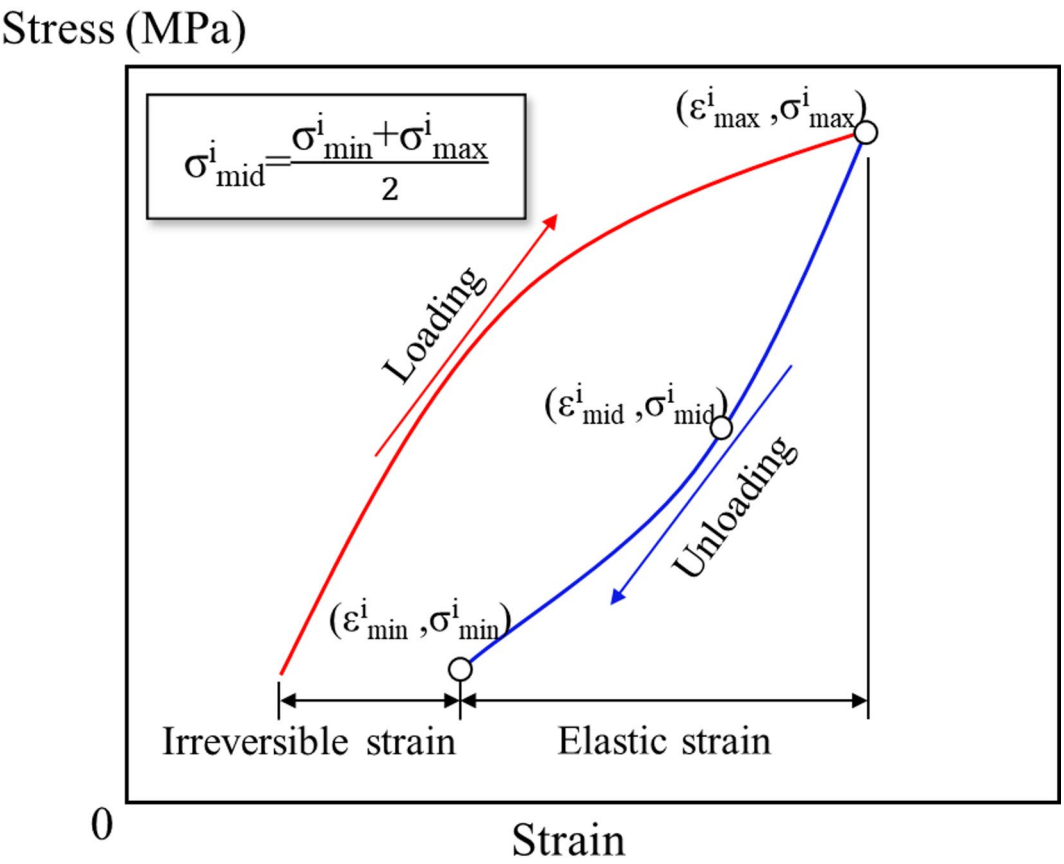

Fig. 6. Calculation method of strain-related parameters.

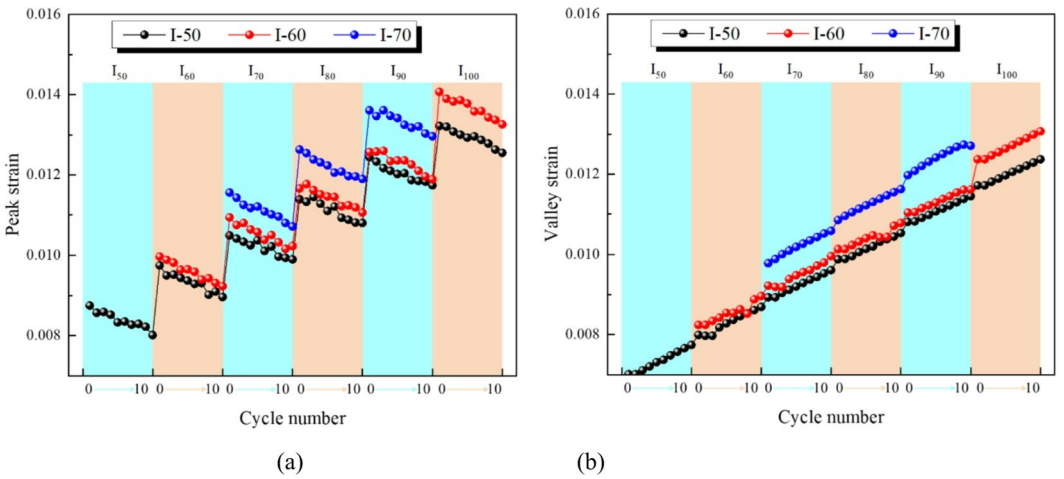

Fig. 7. Peak strain and valley strain of cyclic loading and unloading at different initial stresses: (**a**) Peak strain, (**b**) Valley strain.

Figure 9a also shows that in the stages preceding failure, the irreversible strain of each stage tends to decrease, suggesting a hardening effect in these cyclic stages. With higher initial cyclic stress levels, the coal samples experience fewer cyclic stages with a hardening effect, and their peak strength and brittleness gradually diminish. Therefore, in the failure stage, the higher the initial cyclic stress level, the more pronounced the deformation of the sample, which is evident in the last stage of the curves in Fig. 9a,b.

The particle size distribution of coal samples under different initial stress cyclic loading and unloading can reflect the degree of coal sample damage[33]. In the analysis process, the coal sample fragments with a maximum length of less than 12.5 mm (d < 12.5 mm) are defined as small blocks, the coal sample fragments with a maximum

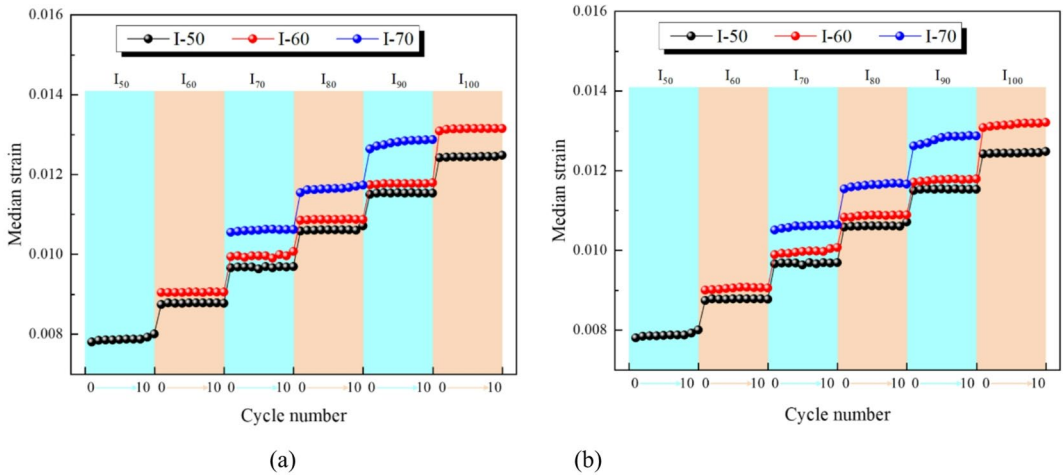

Fig. 8. Peak-median strain of cyclic loading and unloading at different initial stresses: (**a**) Loading stage, (**b**) Unloading stage.

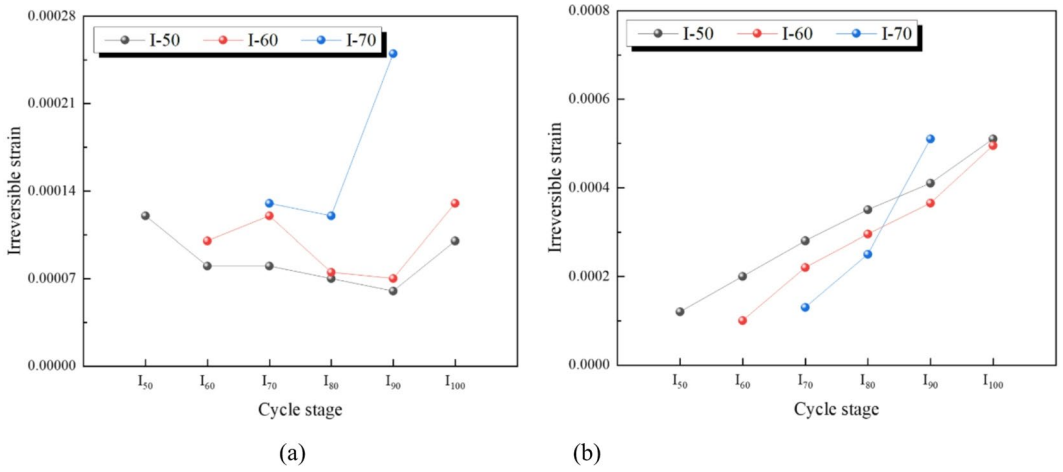

Fig. 9. The irreversible strain evolution characteristics of cyclic loading and unloading process: (**a**) Cumulative irreversible strain of stage, (**b**) Cumulative irreversible strain of cycle.

length of 12.5 to 50 mm ($12.5 \le d < 50$ mm) are defined as medium blocks, and the coal sample fragments with a maximum length greater than or equal to 50 mm ($d \ge 50$ mm) are defined as large blocks. Figure 10a–c shows the particle size and mass fraction distribution of three groups of coal samples under different initial cyclic stress levels. It can be seen that the difference between the coal sample fragments with $d \ge 12.5$ mm in the 70% F_{UCS} and 60% F_{UCS} groups is large and the discreteness is strong, while the difference between the coal sample fragments in the 50% F_{UCS} group is small and the distribution is more uniform. At the same time, the mass fraction of all coal samples shows an increasing trend with the increase of particle size. Obviously, the proportion of the mass of the bulk in the total mass is always the highest when the coal sample is broken, and with the increase of the initial stress level, the distribution of the mass fraction of the coal sample is more concentrated in the larger part of the particle size. This shows that the failure mode of coal samples under low initial cyclic stress level is a multi-crack failure mode of large-scale fracture, while under high initial cyclic stress level is a single-crack failure mode of small-scale fracture. The transformation of the failure mode is also in line with the stage obtained in the previous section, that is, with the increase of the initial cyclic stress level, the brittleness of the coal sample is also smaller, and the crack tends to be a uniform single crack with a small degree of fracture.

In addition, the influence of initial cyclic stress level on the crushing degree of coal samples is analyzed from the perspective of different mass fractions of fragments. First of all, it needs to be clear that the mass fraction of coal sample fragments can reflect the integrity of coal sample crushing. The higher the mass fraction of the small block, the worse the integrity of the coal sample when it is destroyed. Figure 11 horizontally compares the mass distribution of large and small blocks with different initial stress levels. The mass proportions of large and small blocks in the 50% F_{UCS} group are 64% and 22%, respectively. The mass proportions of the 60% F_{UCS} group and the 70% F_{UCS} group are 75% and 19%, 76% and 14%, respectively. From Fig. 11, it can be seen that

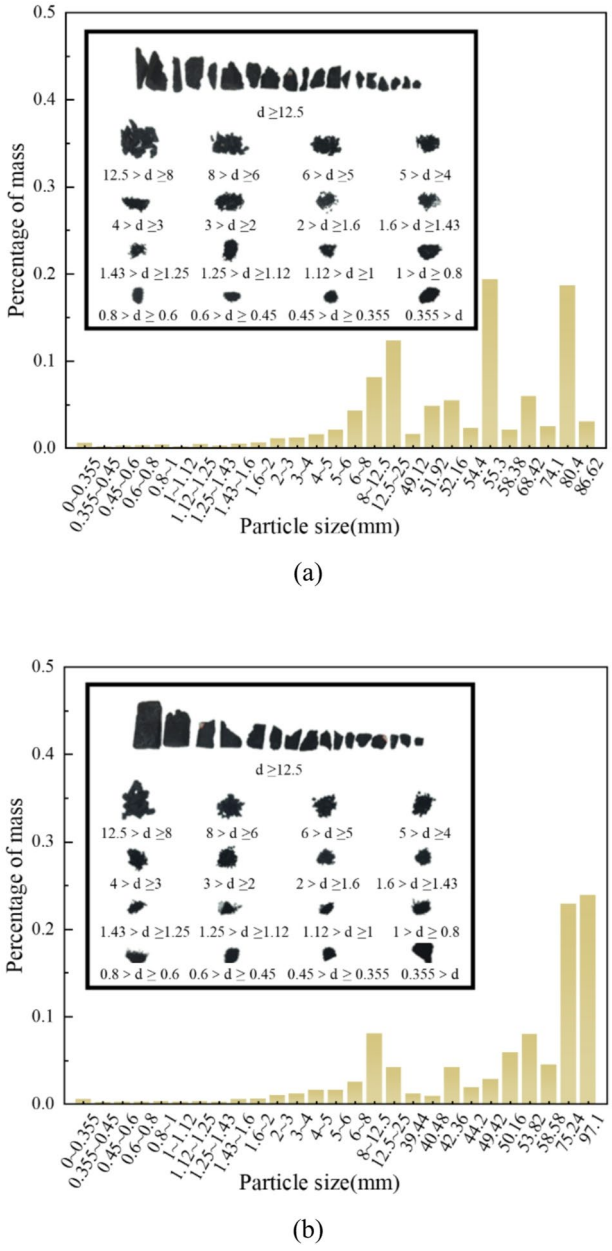

Fig. 10. Distribution of particle size and mass fraction of coal sample fragments: (**a**) I-50, (**b**) I-60, (**c**) I-70.

with the increase of the initial cyclic stress level, the mass proportion of large blocks gradually increases and the mass proportion of small blocks gradually decreases, that is, the increase of the initial stress level will enhance the integrity of the coal sample when it is broken. This phenomenon further illustrates that different initial cyclic stress levels will affect the fracture development during loading. Under the higher initial cyclic stress level, there are fewer cracks in the coal sample during the cyclic loading and unloading process, so there are more large blocks when crushing, and the mass ratio is higher, and the integrity of the coal sample is better.

Energy evolution characteristics

The deformation and damage of rock are driven by energy. The total strain energy represents the total energy input by the mechanical device into the coal sample during the loading process. The elastic strain energy is the energy absorbed by the coal sample when elastic strain occurs; this energy can be released through deformation recovery during unloading. In contrast, the plastic strain energy is the energy absorbed when plastic deformation occurs in the rock. This energy is not released during unloading and is therefore also referred to as dissipative energy. An increase in dissipative energy reflects the ongoing development of micro-defects in the coal, a reduction in strength, and the process leading to ultimate failure. During each cycle of loading, the total energy input from external sources is equal to the sum of the accumulated elastic energy in the coal and the dissipative energy used for fracture development and propagation.

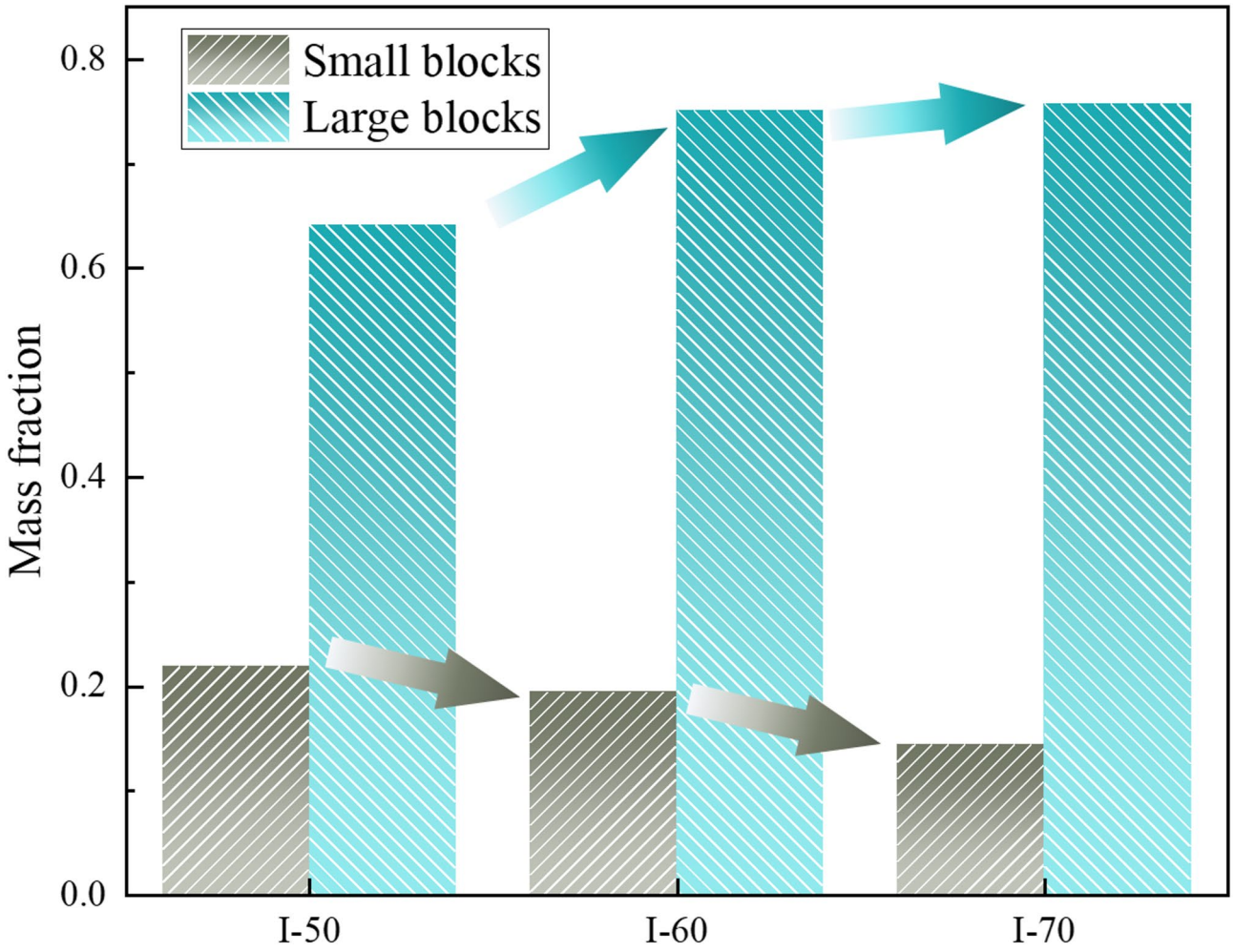

Fig. 11. Mass distribution of large and small blocks under different initial stresses.

The energy evolution characteristics of cyclic loading and unloading on coal under different stress levels are shown in Fig. 12. It can be observed that the proportion of elastic energy in the total energy is significantly higher than that of dissipative energy. This indicates that most of the total energy input into the coal sample during the loading process is stored as elastic energy. Meanwhile, as the number of cycles increases, the proportion of dissipative energy shows an increasing trend. This suggests that, as the cycle progresses, the elasticity of the coal sample gradually decreases, and it exhibits more plastic characteristics, meaning that a greater portion of the absorbed energy contributes to crack development.

With the progression of the loading cycles, the proportion of dissipative energy consistently decreases significantly from the end of one cycle to the beginning of the next. Additionally, the figure shows that the proportion of dissipative energy sharply increases in the final cycle before the coal sample fails, and this sudden increase becomes smaller as the initial cyclic stress level rises. This behavior occurs because the amplitude of each cyclic loading in this experiment's stress path is always greater than the amplitude of unloading, and the unloading is not complete. Due to incomplete unloading, some elastic energy remains stored in the coal sample after each cycle. As the initial cyclic stress level decreases, the coal sample undergoes more cycles, leading to more elastic energy being retained due to incomplete unloading. Consequently, energy release is more intense when failure occurs.

Figure 13 illustrates the evolution characteristics of the cumulative dissipated energy in each cycle stage and across all previous stages during the cyclic loading and unloading process. During this process, the dissipated energy typically first contributes to the closure of the original micro-cracks in the coal sample. As the cracks gradually close, the amount of dissipated energy decreases. Subsequently, the dissipated energy is mainly consumed through plastic deformation and remains stable during this phase. Finally, when the coal sample approaches failure, the dissipated energy primarily facilitates the formation, development, and propagation of new micro-cracks.

In this experiment, the coal sample undergoes a 10-minute stable load-holding stage before the start of cyclic loading and unloading. During this holding period, the micro-cracks generated by the initial loading of the coal sample are compacted. Consequently, during the cyclic stages, less dissipated energy is used for the closure of

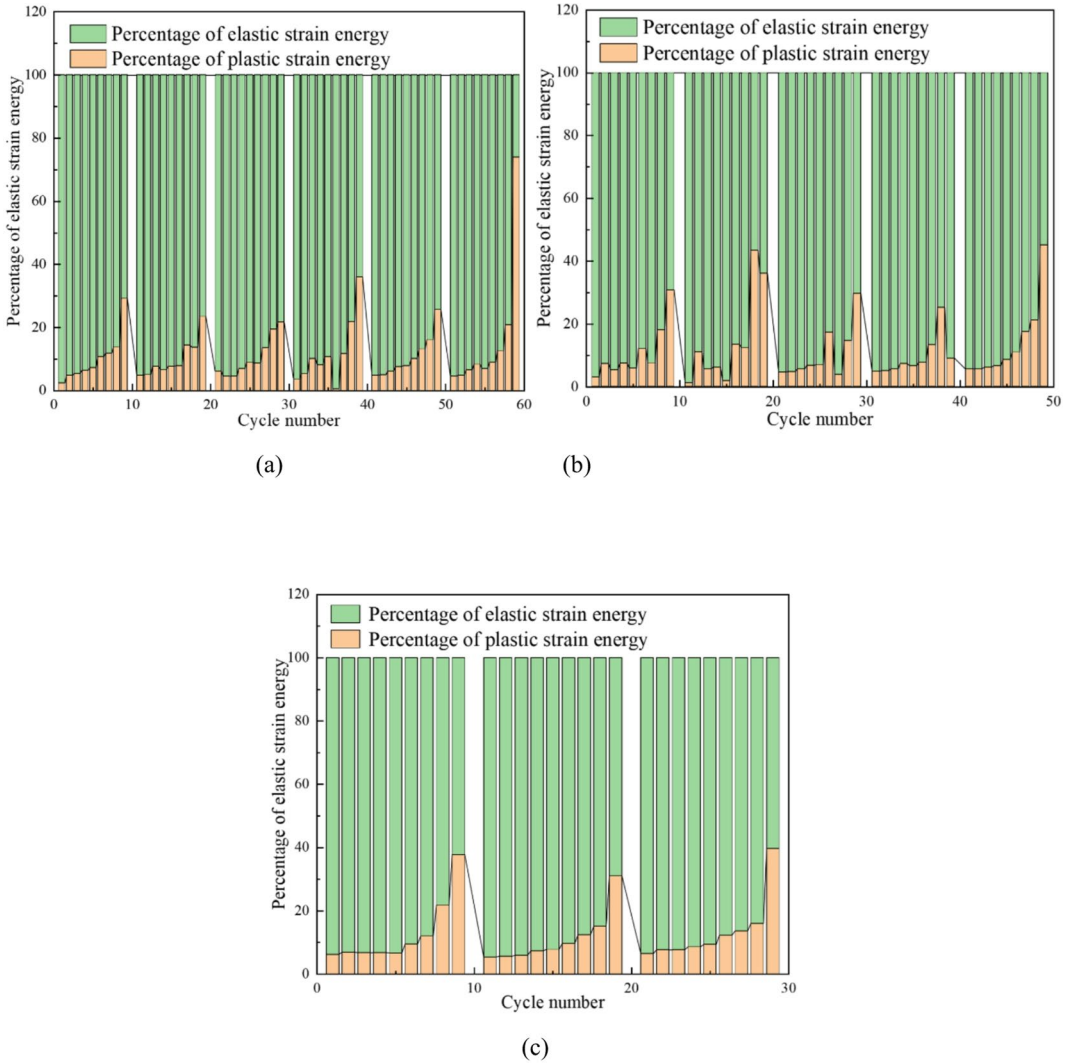

Fig. 12. Proportion of elastic energy and dissipated energy of different samples: (**a**) 50% F_{UCS}, (**b**) 60% F_{UCS}, (**c**) 70% F_{UCS}.

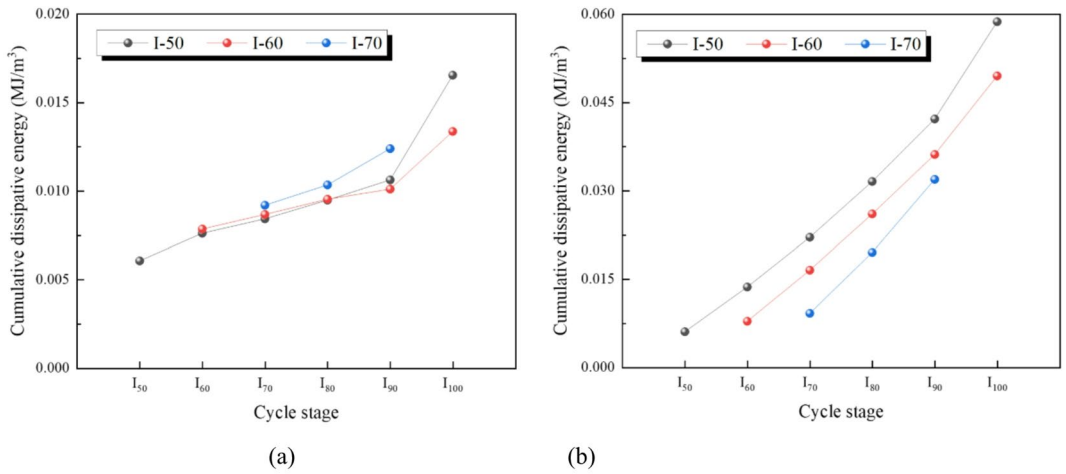

Fig. 13. The evolution characteristics of dissipated energy in cyclic process: (**a**) Stage cumulative dissipated energy, (**b**) Cycle cumulative dissipated energy.

micro-cracks, while more is directly expended on the plastic deformation of the coal sample and the generation, development, and propagation of new fractures.

The cumulative dissipated energy in each stage shows a pattern of gradually increasing, followed by a sudden increase just before failure. Therefore, a significant rise in cumulative dissipated energy during the cyclic stage can also be useful in predicting the failure of coal samples.

Hardening damage mechanism of coal under semi-wetting cyclic loading

Underground reservoirs use coal mining goafs for water storage, with protective coal pillars and artificial dams as structures, aiding coal-water resource coordination. Adjacent mining may disturb pillars, causing fractures and failure. Geological/mining factors affect pillars, akin to cyclic loading/unloading of semi-wet coal with varying initial stress. Studying their fracture/strength traits here is key to predicting pillar dam stability.

During the process of cyclic loading and unloading, two behaviors occur simultaneously in coal rock: the slow compaction of existing cracks and the formation of new cracks. Existing research has demonstrated that these two behaviors lead to hardening and damage effects, respectively, on the coal rock[20]. The dominance of these effects is determined by the loading stress level, and as the stress level increases, the damage effect gradually becomes stronger than the hardening effect.

Based on the observation that the uniaxial compressive strength under different initial cyclic stress levels in this experiment is greater than the uniaxial compressive strength under conventional loading, it can be concluded that the three cyclic stages, I_{50}, I_{60}, and I_{70}, are primarily loading processes dominated by the hardening effect. A lower initial cyclic stress level means that the coal sample is subjected to more cycles dominated by the hardening effect, which requires more energy dissipation for failure. This also explains the gradual decrease in cumulative dissipated energy from another perspective. At the same time, because the cumulative irreversible strain increases from the I-60 coal sample to the I-70 coal sample, it indicates that the I-70 coal sample generates more new cracks during a certain cyclic loading and unloading process. Combined with the change in the cumulative irreversible strain of the I-70 coal sample in a single cycle stage, it can be determined that more new cracks are generated in the I_{90} cycle stage, indicating that this cycle stage is dominated by the damage effect. Additionally, it should be noted that for the I-80 and I-90 coal samples, the stage with more new crack formation is the I_{100} stage. This suggests that a lower initial cyclic stress level can increase the critical threshold for transitioning from the strengthening effect to the damage effect, as shown in Fig. 14.

Furthermore, the cyclic stages dominated by the hardening effect, as mentioned in the above analysis, can also increase the brittleness of the coal samples. Therefore, coal samples with a higher initial cyclic stress level undergo fewer hardening cycles, resulting in lower brittleness and greater plastic deformation at the point of failure, with the cracks being more uniform and singular. This also explains the phenomenon that coal samples with a higher initial cyclic stress level have a greater mass of larger blocks and a lower mass of smaller blocks at the time of failure.

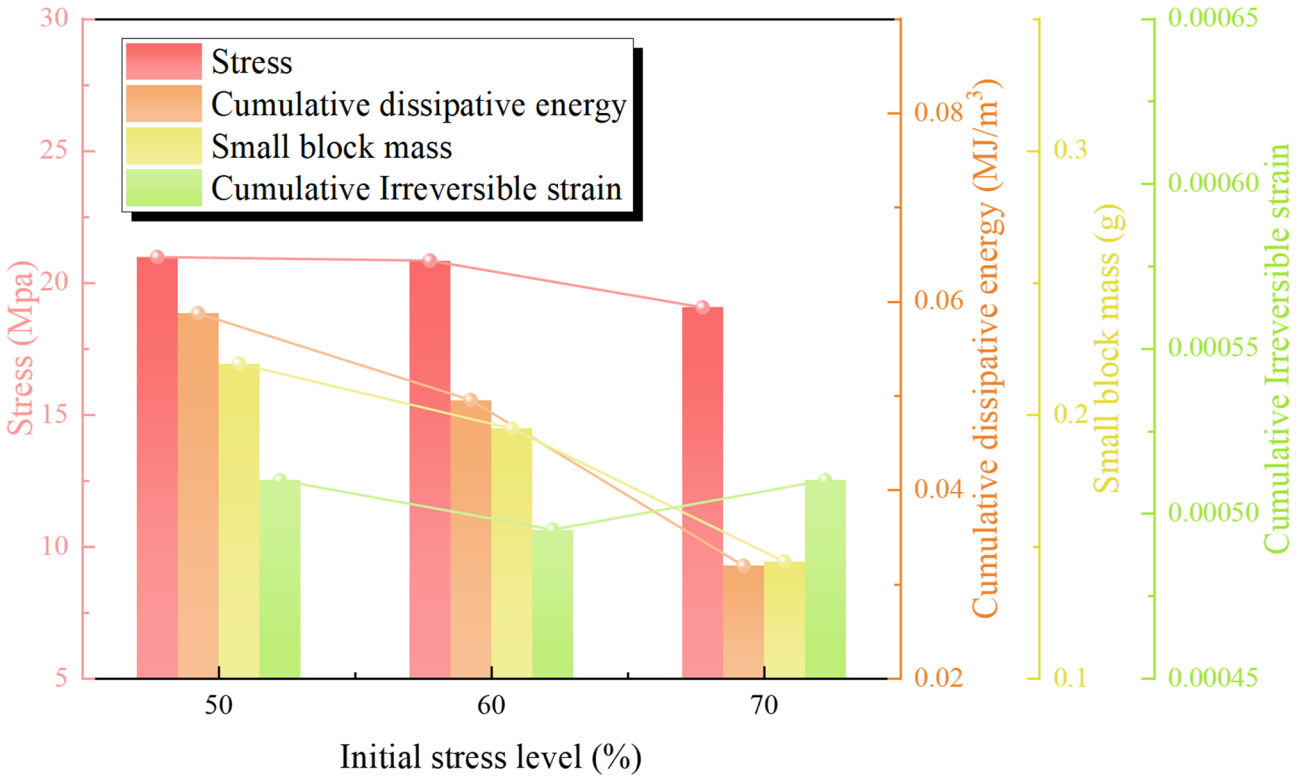

Fig. 14. Relationship between several parameters.

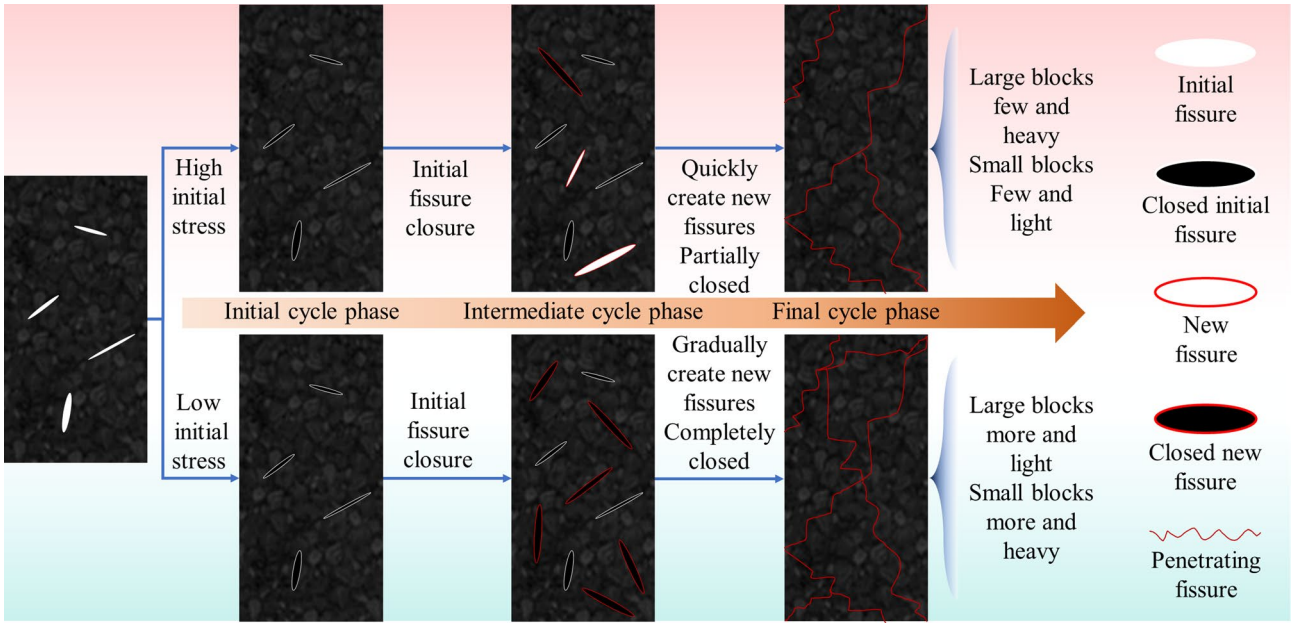

Fig. 15. Damage and hardening law of coal samples under different initial cyclic stress levels.

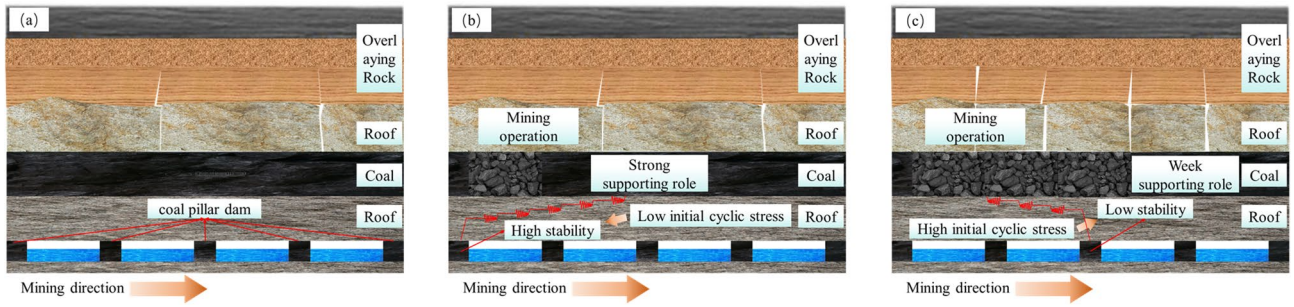

Fig. 16. Schematic diagram of unstable area identification mechanism of coal pillar dam: (**a**) Typical underground reservoir configurations. (**b**) Low initial cyclic stress condition. (**c**) High initial cyclic stress condition.

Under the action of stress disturbance, the coal pillars in the water storage goaf will continually undergo the closure of existing cracks and the formation of new cracks before failure. As a component of the underground reservoir dam, changes in the fracture patterns of the coal pillar directly affect the stability and safety of the dam. Therefore, it is essential to consider the impact of different initial cyclic stress levels on the variation in fracture propagation and closure.

Based on the previous analysis of the strain, particle size, and mass ratio of coal samples after failure, the damage and hardening behaviors of coal samples under different initial cyclic stresses can be determined, as shown in Fig. 15. It can be observed from the diagram that, under lower initial stress, the coal sample tends to develop more new cracks during the middle stages of the cycle; however, these new cracks are quickly closed again due to cyclic loading and unloading soon after they form. Additionally, during cycles at this stress level, the coal sample produces more small coal fragments. These fragments are small in size and can block existing cracks in the coal, further reducing crack space, promoting crack closure, and increasing strength and brittleness, thereby improving the stability of the coal pillar dam.

Conversely, under higher initial stress, newly generated cracks in the coal sample are less likely to close promptly, and the sample is more prone to form large blocks during cycles at this stress level, which further hinder crack closure. This condition is more likely to lead to a decrease in the strength of the coal sample, an increase in failure deformation, and a reduction in the stability of the coal pillar dam.

The identification of unstable zones in coal pillar dams is critically important based on the revealed "stress-level dependent hardening-damage transition" mechanism, as illustrated in Fig. 16. In typical underground reservoir configurations (Fig. 16a), coal pillar dams coexist with one or more unmined working faces in adjacent coal seams. When mining operations approach the reservoir area (Fig. 16b), the relatively short advance distance and strong support from remnant coal seams result in low initial stress levels in nearby coal pillar dams. Under

these conditions, the hardening effect predominates, significantly enhancing structural stability. As mining progresses further (Fig. 16c), the increasing advance distance progressively reduces support from remnant coal seams, ultimately leading to more pronounced overburden roof collapse, which collectively elevates the initial stress levels experienced by nearby coal pillar dams during cyclic loading. This stress increase triggers the damage-dominated regime that substantially compromises stability. This study systematically investigates the hardening-damage transition mechanism across different initial cyclic stress levels and quantitatively evaluates its impact on the positional stability variations of coal pillar dams.

Conclusions

This study examined the strength and elastic modulus of coal samples subjected to varying initial cyclic stresses under decreasing-amplitude cyclic loading, under identical soaking conditions. The study also analyzed the deformation behavior under different initial cyclic stresses and characterized the particle size and mass distribution patterns after failure Additionally, the energy evolution process of coal samples throughout these conditions was investigated. The research findings provide theoretical support for the design of coal pillar dams in the goaf of underground reservoirs in coal mines. The main conclusions are as follows:

(a) The strength and elastic modulus of coal samples decrease as the initial cyclic stress level increases; however, compared to the conventional uniaxial compressive strength, the strength of the coal samples under this experimental condition is enhanced. This indicates that a certain degree of cyclic loading and unloading can improve the strength of coal samples, but as the initial cyclic stress level increases, the strengthening effect and resistance to deformation reduces.
(b) The distribution of particle size and mass distributions of coal samples after failure is also related to the initial cyclic stress level. As the initial cyclic stress level increases, fewer small blocks are produced, and more large blocks are generated. The formation of small blocks is more conducive to filling internal cracks in the coal samples, thereby improving their elasticity.
(c) Across all cycle stages, the dissipated energy of different coal samples consistently shows an increasing trend. This indicates that as the cycles progress, the elasticity of the coal samples gradually decreases, and they exhibit more plastic characteristics, meaning that a greater portion of the absorbed energy contributes to crack development. As the initial cyclic stress level increases, the cumulative dissipated energy of the coal samples in a single stage shows an increasing trend, but the total cumulative dissipated energy displays a downward trend.
(d) Under cyclic loading, both the compaction of existing cracks and the formation of new cracks occur within the coal sample. At lower initial cyclic stress levels, the degree of crack compaction and closure is higher, and the small fragments generated inside the coal sample help block and fill these cracks, enhancing the strength and elasticity of the coal while also increasing its brittleness. This results in a stronger coal pillar that is more resistant to failure, with reduced deformation at the point of failure, which is advantageous for the coal pillar when used as a reservoir dam. Conversely, at higher initial cyclic stress levels, the degree of crack compaction and closure is lower, leading to greater deformation and reduced strength. Therefore, the stability of the coal pillar is diminished under high initial cyclic stress levels, making it more likely to become the weak point of the reservoir dam.

Data availability

All data, models, and code generated or used during the study are included in the submitted article.

Received: 19 September 2024; Accepted: 9 September 2025
Published online: 10 October 2025

References

1. Xie, H. P. et al. New concept of coal revolution and conception of coal science and technology development. *J. China Coal Soc.* **43**, 1187–1197 (2018).
2. Green, F. & Stern, N. China's changing economy: implications for its carbon dioxide emissions. *Clim. Policy*. **17**, 423–442 (2017).
3. Liu, C. S. et al. Allocation and utilization of coal mine water for ecological protection of lakes in semi-arid area of China. *Sustainability*. **14**, 18 (2022).
4. Yang, G. Y. et al. The relationship between China's coal resource development and water resource. In *Proceedings of the 7th International Conference on Applied Energy (ICAE), Abu Dhabi, U. Arab Emirates, Mar 28–31, 2015* (Elsevier Science BV, 2015).
5. Gu, D. Z. Theory framework and technological system of coal mine underground reservoir. *J. China Coal Soc.* **40**, 239–246 (2015).
6. Yuan, L. et al. Precision exploitation and utilization of closed/abandoned mine resources in China. *J. China Coal Soc.* **43**, 14–20 (2018).
7. Xie, H. P. et al. New technology of pumped storage power generation in underground coal mine: principle, present situation and prospect. *J. China Coal Soc.* **40**, 965–972 (2015).
8. Gu, D. Z. et al. Experimental study and numerical simulation for dynamic response of coal pillars in coal mine underground reservoir. *J. China Coal Soc.* (2016).
9. Zhang, Y. et al. Seismic safety analysis of interlaminar rock mass in the distributed underground reservoir of a coal mine. *Water* **16**, 19 (2024).
10. Pan, Y. S. & Wang, A. W. Disturbance response instability theory of rock bursts in coal mines and its application. *Geohazard Mech.* **1**, 1–17 (2023).
11. Ma, Q. et al. Monitoring and evaluation of disaster risk caused by linkage failure and instability of residual coal pillar and rock strata in multi-coal seam mining. *Geohazard Mech.* **1**, 297–307 (2023).
12. Qiao, P. et al. Simulation of underground reservoir stability of pumped storage power station based on fluid-structure coupling. *CMES-Comp Model. Eng. Sci.* **139**, 1381–1399 (2024).
13. Wang, X. et al. Deformation and acoustic emission characteristics of coal with different water saturations under Cyclic load. *Soil. Dyn. Earthq. Eng.* **162**, 14 (2022).

14. Gao, X. C. et al. Development of a DEM-based method for modeling the water-induced failure process of rock from laboratory- to engineering-scale. *Int. J. Geomech.* **20**, 14 (2020).
15. Wong, L. N. Y., Maruvanchery, V. & Liu, G. Water effects on rock strength and stiffness degradation. *Acta Geotech.* **11**, 713–737 (2016).
16. Cai, G. Q. et al. Experimental study on tensile strength of unsaturated fine sands. *Acta Geotech.* **15**, 1057–1065 (2020).
17. Wang, W. N. et al. Experimental study on the shear characteristics and weakening mechanism of water-bearing rock joints. *Bull. Eng. Geol. Environ.* **80**, 7653–7668 (2021).
18. Zhang, Z. Z. & Gao, F. Experimental investigation on the energy evolution of dry and water-saturated red sandstones. *Int. J. Min. Sci. Technol.* **3**, 6 (2015).
19. Yao, Q. L. et al. Experimental investigation of the mechanical failure behavior of coal specimens with water intrusion. *Front. Earth Sci.* **7**, 13 (2020).
20. Vishal, V., Ranjith, P. G. & Singh, T. N. An experimental investigation on behaviour of coal under fluid saturation, using acoustic emission. *J. Nat. Gas Sci. Eng.* **22**, 428–436 (2015).
21. Perera, M. S. A., Ranjith, P. G. & Peter, M. Effects of saturation medium and pressure on strength parameters of Latrobe Valley brown coal: carbon dioxide, water and nitrogen saturations. *Energy* **36**, 6941–6947 (2011).
22. Pan, Z. J. et al. Effects of matrix moisture on gas diffusion and flow in coal. *Fuel* **89**, 3207–3217 (2010).
23. Peng, K., Zhou, J. Q. & Zou, Q. L. Deformation characteristics and failure modes of sandstones under discontinuous multi-level Cyclic loads. *Powder Technol.* **373**, 599–613 (2020).
24. Feng, F. et al. Analysis of fractures of a hard rock specimen via unloading of central hole with different sectional shapes. *Energy Sci. Eng.* **7**, 2265–2286 (2019).
25. Peng, K., Zhou, J. Q. & Zou, Q. L. Deformation behavior of sandstones during multilevel Cyclic loading and unloading under varying lower stress limits: effect of stress amplitude and underlying mechanism. *Int. J. Geomech.* **22**, 17 (2022).
26. Meng, Q. B. et al. Effects of acoustic emission and energy evolution of rock specimens under the uniaxial Cyclic loading and unloading compression. *Rock. Mech. Rock. Eng.* **49**, 3873–3886 (2016).
27. Song, Z. Y. et al. Mechanical and microseismic characteristics of sandstones subject to moderate low-frequency differential Cyclic loading (DCL) followed by monotonic loading up to failure. *Acta Geotech.* **18**, 187–215 (2023).
28. Liang, Y. P., Ran, Q. C. & Zou, Q. L. Experimental study of mechanical behaviors and failure characteristics of coal under true triaxial Cyclic loading and unloading and stress rotation. *Nat. Resour. Res.* **31**, 971–991 (2022).
29. Liu, Q. H. et al. Failure characteristics of the water-resisting coal pillar under stress-seepage coupling and determination of reasonable coal pillar width. *Water* **15**, 22 (2023).
30. Tan, T. J., Wang, E. Y. & Wang, X. R. Resistivity and damage of coal under Cyclic loading and unloading. *Eng. Geol.* **323**, 11 (2023).
31. ISRM The complete ISRM. Suggested methods for rock characterization, testing and monitoring: 1974–2006. In: Ulusay R, Hudson JA (eds) Suggested Methods Prepared by the Commission on Testing Methods, International Society for Rock Mechanics, Compilation Arranged by the ISRM Turkish National Group. Kozan Ofset, Ankara (2007).
32. Zheng, Z. et al. Microdynamic mechanical properties and fracture evolution mechanism of Monzogabbro with a true triaxial multilevel disturbance method. *Int. J. Min. Sci. Technol.* **34**, 385–411 (2024).
33. Zou, Q. L. et al. Morphological evolution and flow conduction characteristics of fracture channels in fractured sandstone under Cyclic loading and unloading. *Int. J. Min. Sci. Technol.* **33**, 1527–1540 (2023).

Acknowledgements

This work was supported by Open Fund of State Key Laboratory of Water Resource Protection and Utilization in Coal Mining (Grant No. GJNY-20-113-01), and the National Natural Science Foundation of China (No.52404109), which were gratefully acknowledged.

Author contributions

F.L., F.K., and Q.Z. made substantial contributions to the conception and design of the work, as well as the acquisition, analysis, and interpretation of data. Y.Z., and X.L. drafted the manuscript and critically revised it for important intellectual content. All authors have approved the final version for publication.

Declarations

Competing interests

The authors declare no competing interests.

Additional information

Correspondence and requests for materials should be addressed to F.K.

Reprints and permissions information is available at www.nature.com/reprints.

Publisher's note Springer Nature remains neutral with regard to jurisdictional claims in published maps and institutional affiliations.